

Water Induced Structural Transformations in Flexible Two-Dimensional Layered Conductive Metal–Organic Frameworks

Yuliang Shi, Mohammad R. Momeni,* Yen-Jui Chen, Dil K. Limbu, Zeyu Zhang, and Farnaz A. Shakib*



Cite This: *Chem. Mater.* 2022, 34, 7730–7740



Read Online

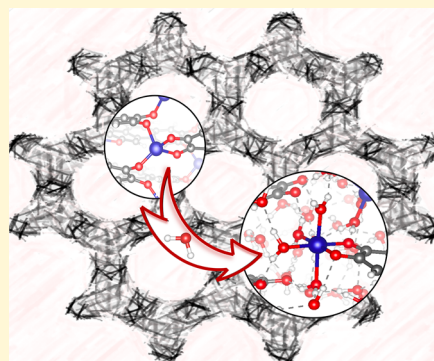
ACCESS |

Metrics & More

Article Recommendations

Supporting Information

ABSTRACT: The flexible and ever-changing layered structure of electrically conductive 2D metal–organic frameworks (MOFs) poses a formidable challenge for establishing any structure–application relationships. Here, we employ a combined quantum mechanics and classical molecular dynamics (MD) approach allowing large-scale/long-time simulations of the dynamics of both dry and hydrated systems to investigate the intrinsic flexibility and dynamical motions of layered 2D MOFs and its effect on their physical and chemical properties. The $\text{Co}_3(\text{HHTP})_2$ and $\text{Cu}_3(\text{HHTP})_2$ [HHTP = 2,3,6,7,10,11-hexahydroxytriphenylene] MOFs as two representatives of the layered family of MOFs are studied in great details with a focus on their experimentally observed differential framework stabilities in aqueous solutions. Our MD simulations reproduce structural properties of both MOFs as well as a higher tendency of the $\text{Co}_3(\text{HHTP})_2$ MOF towards water attack and hydrolysis than its $\text{Cu}_3(\text{HHTP})_2$ counterpart, in agreement with available experimental reports. The results show the presence of two distinctive metastable metal centers with (pseudo)planar vs (pseudo)tetrahedral configurations where the latter are more positively charged than the former and hence more susceptible to water nucleophilic attacks. The accurate $\omega\text{B97M-v}$ quantum-mechanical calculations show the higher tendency of the open Co^{2+} sites for coordination to water molecules than the open Cu^{2+} sites. Our multifaceted strategy paves the way towards simulation of realistic MOF-based materials and their interface with confined water molecules which is especially relevant to designing more robust water stable materials with desired properties and applications.



INTRODUCTION

The discovery of graphene and its derivatives^{1,2} brought two-dimensional (2D) materials to the center of attention. Due to fascinating structural and electrical features, these materials are considered as unlimited rising stars for future materials engineering.^{3–8} Conductive layered metal–organic frameworks (MOFs)⁹ are a new family of 2D materials which offer electrical conductivity^{10–13} in addition to other known properties of MOFs, including permanent porosity and exceptionally high surface area.^{14–16} Thanks to the ideal architecture and electrical properties of 2D MOFs, unprecedented breakthroughs are on the horizon, in producing high-performance and cost-effective semiconductors,^{17,18} supercapacitors,^{19–22} and ion-to-electron transduced chemical sensors.^{23–33} Making progress towards these applications depends on a deep understanding of structural, electronic, and dynamical behavior of 2D MOFs at atomistic levels. Specifically, since 2D MOFs could be utilized as semiconductors and supercapacitors, their structural stability subject to humidity should be fully understood. As electrochemical sensors, 2D MOFs might be required to operate in aqueous solutions which calls for a full investigation of possible hydrolysis of the MOF secondary building unit (SBU) and its effects on the structural integrity and electrical conductivity of the whole layered architecture. In fact, hydrolysis of SBUs is a known phenomenon since the very first experimental report of

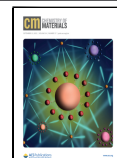
2D MOFs. In 2012, Yaghi and co-workers prepared the first family of these layered materials via linking conjugated 2,3,6,7,10,11-hexahydroxytriphenylene (HHTP) linkers with Co(II), Cu(II), and Ni(II) metal centers into 2D extended sheets (**Figure 1a**).⁹

The reported crystallographic data hinted on different layered architectures of these MOFs in the presence of water.⁹ Two independent metal sites were found for Ni(II) and Co(II), referring to alternate distinct layers. In one layer, metal atoms are coordinated to two adjacent HHTP linkers and two axial water molecules to form $\text{M}_3(\text{HHTP})_2(\text{H}_2\text{O})_6$ layers (**Figure 1b**), whereas in the other, the conjugated nature of layers is disrupted, and metal atoms are coordinated to one linker and four water molecules to form $\text{M}_3(\text{HHTP})(\text{H}_2\text{O})_{12}$ complexes (**Figure 1c**). On the other hand, Cu^{2+} forms only one type of metal center and creates a uniform structure composed of fully conjugated $\text{Cu}_3(\text{HHTP})_2(\text{H}_2\text{O})_6$ layers (**Figure 1b**). This is only one example of many open questions

Received: March 31, 2022

Revised: July 13, 2022

Published: August 16, 2022



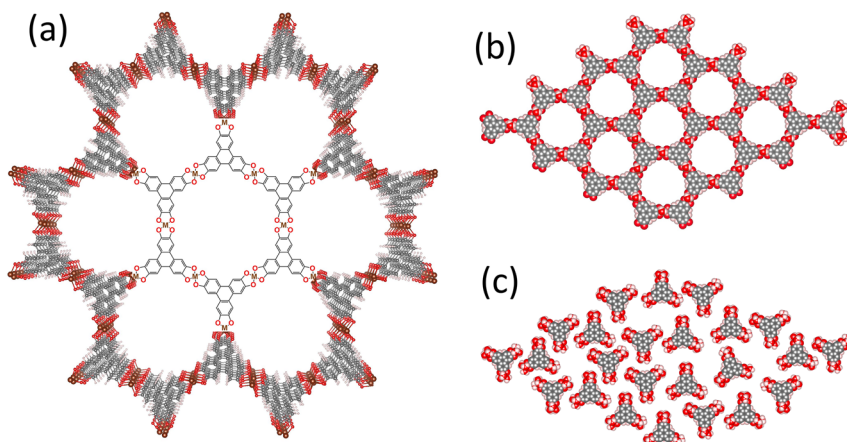


Figure 1. (a) General extended structure of 2D $M_3(\text{HHTP})_2$ MOFs along 1D channels where $M = \text{Cu}^{2+}$ and Co^{2+} are connected to $\text{HHTP} = 2,3,6,7,10,11\text{-hexahydroxytriphenylene}$ linkers. Aqueous solution experiments by Hmudeh et al.⁹ show the presence of $M_3(\text{HHTP})_2(\text{H}_2\text{O})_6$ (b) and $M_3(\text{HHTP})(\text{H}_2\text{O})_{12}$ (c) layers for $M = \text{Co}^{2+}$ but only $M_3(\text{HHTP})_2(\text{H}_2\text{O})_6$ for $M = \text{Cu}^{2+}$.

on how structural features determine the water stability, chemical reactivity, and electrical conductivity of 2D MOFs which themselves display constant structural dynamics. Displacement of layers compared to each other (slipping), as evidenced by experimental and simulated powder X-ray results,¹⁷ is the most established dynamical feature of these MOFs. We emphasize that dynamical flexibility is an intrinsic characteristic of 2D π -stacked layered MOFs which should be investigated and addressed before any defect/deformation or dopant engineering strategy can be employed for tuning the electrical conductivity of these materials.^{34,35} Conducting such a study with *ab initio* molecular dynamics (AIMD) simulations, where the energies and forces felt by the nuclei are calculated “on-the-fly” with an electronic structure method, is prohibitively expensive. Currently, typical time and length scales that are accessible with AIMD are up to hundreds of femtoseconds to tens of picoseconds, and up to a few hundreds of atoms. It becomes even more challenging when solvent (water) is present which can create an interface with the framework. This calls for longer simulation times, on the order of nanoseconds, to sample the entire phase space given the fact that reorientation relaxation time of H_2O molecules in bulk water, i.e., the amount of time it takes for water to break its hydrogen bond and form another one, is ~ 2 ps.^{36–38} In response to this challenge, here we develop *ab initio* force fields (AIFFs) specifically parametrized for $\text{Cu}_3(\text{HHTP})_2$ and $\text{Co}_3(\text{HHTP})_2$ MOFs for large-scale and long-time MD simulations with reasonable accuracy.

With the help of these simulations, we demonstrate different degrees of flexibility of 2D MOFs that result in a range of interesting structural dynamics including (i) slipping of layers compared to each other, (ii) expansion/contraction of layers along the stacking direction, and (iii) deformation of triphenylene organic linkers. Moreover, the hexagonal 1D channels of 2D MOFs provide for interesting mechanical confinement effects that can potentially induce substantial changes on different thermodynamic and dynamical properties of confined water molecules. Studying the behavior of water confined in the cavities and channels of different porous materials has been the subject of a wide range of theoretical and experimental studies. Dynamics and adsorption of confined water have been widely studied in carbon nanotubes,^{39,40} zeolitic imidazolate frameworks (ZIFs),^{41,42}

MOFs,^{43–49} and imogolite nanotubes.⁵⁰ When it comes to 2D MOFs, little experimental data, if not no experimental data, is available on thermodynamics and dynamics of confined water in 1D channels. With the developed AIFFs, we characterize mobility of water with respect to (i) diffusion in 1D channels, (ii) adsorption by forming either hydrogen bonds with organic linkers or coordinative bonds with open-metal sites, and (iii) penetration within the interlayer spaces of these 2D π -stacked layered materials. The dynamical simulations of hydrated MOFs are followed by accurate quantum-mechanical calculations at the $\omega\text{B97M-v}$ level which provide detailed insights on the affinity of Co^{2+} and Cu^{2+} metal centers for coordination to water molecules.

■ THEORY AND COMPUTATIONAL DETAILS

Optimized crystal structures of 2D MOFs at 0 K using conventional static electronic structure methods are too perfect for reflecting the flexible nature of these layered materials. Here, we study 2D MOFs via a combination of cluster and periodic quantum-mechanical calculations and classical molecular dynamics (MD) simulations. We developed flexible *ab initio* force fields (AIFFs) for MD simulations that can provide a more realistic picture of the structural and dynamical properties of 2D MOFs with reasonable accuracy. We give a brief description of our strategy for creating the AIFFs here; the interested reader is referred to the Supporting Information (SI) Section S1 for more details. We started from the experimental crystallographic data available for aqueous $\text{Co}_3(\text{HHTP})_2$ ⁹ and built a $2 \times 2 \times 2$ supercell for the dry MOF by removing hydrolyzed layers, solvent molecules, and all chemisorbed water molecules, and then adjusting the interlayer distance to ~ 4 Å. This supercell was then optimized with periodic boundary conditions. Both cell vectors and atomic positions were minimized using the PBE⁵¹ density functional with damped D3 dispersion correction⁵² in CP2K version 5.1.⁵³ For creating the training sets, reduced SBUs with two catecholate linkers were cut from these optimized supercells (see Figure S1). Electronic energies of the training set were calculated using the $\omega\text{B97M-v}$ ⁵⁴ density functional and the def2-TZVP basis set as implemented in QCHEM 5.2.⁵⁵ David Carroll's genetic algorithm^{56,57} was used to fit all interactions involving the Co^{2+} and Cu^{2+} transition metal centers while all parameters involving the intramolecular

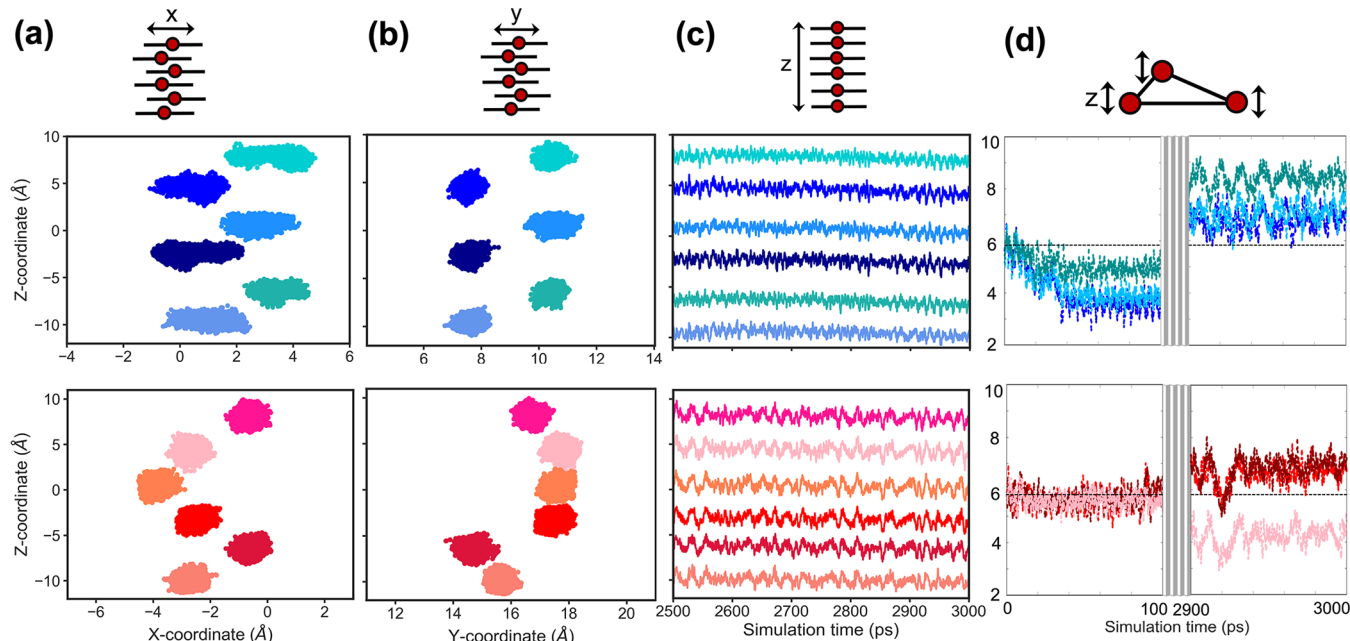


Figure 2. Characterization of different dynamical motions in 2D MOFs with schematic representations, and simulation results for $\text{Co}_3(\text{HHTP})_2$ on the top row (blue) and $\text{Cu}_3(\text{HHTP})_2$ on the bottom row (red). Slipping of six adjacent layers in x (a) and y (b) directions using the positions of six different metal nodes, red circles in the scheme, as a geometrical indicator; vertical movement of six adjacent layers in the z direction (c); and deformation of the linker, illustrated with a black triangle, using the positions of three attached metal nodes as a geometrical indicator (d).

interactions of the organic linkers were taken from generalized amber force field (GAFF).⁵⁸ Morse potentials were used for all coordinative metal-oxo bonds to allow linker displacement and possible hydrolysis in the presence of confined water. The complete list of the bonded and nonbonded parameters for $\text{Cu}_3(\text{HHTP})_2$ and $\text{Co}_3(\text{HHTP})_2$ AIFFs are given in the SI, Tables S1–S5 and S6–S10, respectively, and details of the electronic structure calculations are provided in Section S3. The developed AIFFs were validated against the available experimental data and highly accurate *ab initio* electronic structure calculations (see Section S2 and Figures S2–S6).

Classical MD simulations were performed on $2 \times 2 \times 3$ hexagonal ($a = b = 44.260 \text{ \AA}$, $c = 23.007 \text{ \AA}$, $\alpha = \beta = 90^\circ$, and $\gamma = 120^\circ$) supercells composed of 1512 atoms in total, and 72 metal centers, using our in-house software package DL_Poly Quantum v1.0⁵⁹ which is developed based on DL_Poly Classic v1.10⁶⁰ which is in turn derived from DL_Poly 2.⁶¹ Some of the most important implementations in DL_Poly Quantum v1.0, which are relevant to this work, include (i) implementing the Nosé–Hoover chain (NHC) thermostat for classical simulations in the canonical (NVT) ensemble based on the Suzuki–Yoshida scheme,^{62–64} (ii) implementing the NHC thermostat/barostat for the isothermal–isobaric (NPT) ensemble through the Martyna–Tobias–Klein (MTK) algorithm,^{65,66} and (iii) implementing the four-site flexible water potential model q-TIP4P/F.⁶⁷ The dry MOFs were equilibrated for 3 ns in the NPT ensemble with a time step of 0.2 fs at the experimentally measured temperature and pressure of 293 K and 1 atm. The NHC with 3 thermostats coupled to the MTK barostat as implemented in DL_Poly Quantum was used for all simulations (for simulation details, see Section S4 and Figures S7 and S8). To study dynamics of confined water, starting from the 3 ns MD equilibrated dry MOFs, we randomly packed $2n = 72$, $4n = 144$, $6n = 216$, $8n = 288$, and $10n = 360$ water molecules in the simulation cell using the PACKMOL⁶⁸ code with $n = 36$ being the number of metal

centers in each 1D channel. Each hydrated system was then equilibrated for 2 ns in the NPT ensemble. To model water molecules, we implemented the flexible 4-site q-TIP4P/F⁶⁷ quantum water potential that has been shown to successfully reproduce a diverse number of static and dynamical properties of water including melting point, diffusion coefficients, and IR spectrum. Furthermore, through extensive benchmarking, Manolopoulos and co-workers have shown that classical MD simulations using the q-TIP4P/F water model is an optimal choice to retain reasonable accuracy together with computational efficiency;⁶⁷ the interested reader is referred to Section S5 for more details on this topic. Thermodynamical enthalpies of adsorption for different water contents were calculated from averaging configurational energies over the last 500 ps of the NPT simulations whereas dynamical properties were calculated from the average of 10 independent NVE simulations.

RESULTS AND DISCUSSION

Characterization of Dynamical Motions in 2D MOFs.

First, we explore different structural and dynamical features of the dry $\text{Cu}_3(\text{HHTP})_2$ and $\text{Co}_3(\text{HHTP})_2$ MOFs by analyzing our MD trajectories in the NPT ensemble at 293 K temperature and 1 atm pressure. We find that though both MOFs are vividly flexible with a wide variety of dynamical features, they conserve their perfect layered architecture during the entire 3 ns simulation (see Section S6 and Figures S10 and S11). In close agreement with the previous experimental data, our simulations show that each layer preserves a $\sim 20 \text{ \AA}$ diameter cavity leading to 1D channels being formed along the z direction. The simulated PXRD results of the final snapshot of our MD simulations for $\text{Cu}_3(\text{HHTP})_2$ and $\text{Co}_3(\text{HHTP})_2$ are compared to the experimental PXRD results (see Figure S2), where four prominent peaks corresponding to [100], [200], [130], and [201] reflections show long-range order in the ab plane, i.e., xy direction. Furthermore, very broad and

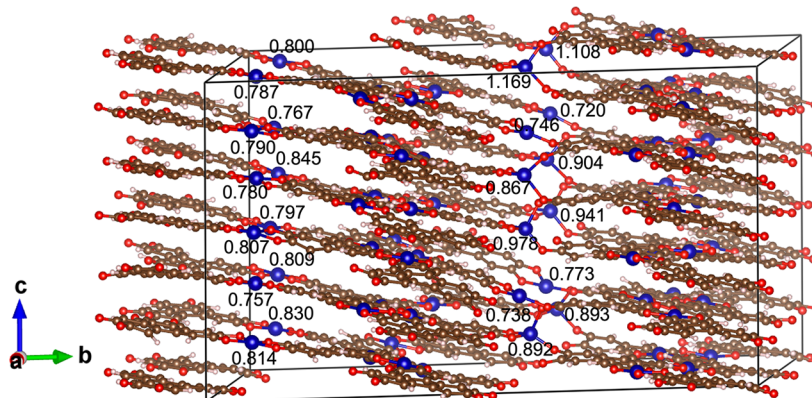


Figure 3. Two different metal–ligand coordination environments in $\text{Co}_3(\text{HHTP})_2$: nearly square planar vs (pseudo)tetrahedral Co centers. The latter sites are characterized as *intrinsic deformation sites* in this work, which are more susceptible to nucleophilic attacks from water molecules as evidenced from our PBE-D3 computed RESP charges shown.

weak peaks at $2\theta = 25.2^\circ$ and 25.5° for $\text{Cu}_3(\text{HHTP})_2$ and $\text{Co}_3(\text{HHTP})_2$, respectively, corresponding to the [001] reflections are indicative of poorer long-range order along the c direction, as expected for van der Waals linked layered materials. Using Bragg's equation the interlayer distances of $\text{Cu}_3(\text{HHTP})_2$ and $\text{Co}_3(\text{HHTP})_2$ are calculated to be $d = 3.53$ and $d = 3.49 \text{ \AA}$, which are in good agreement with the same calculations on experimental PXRDs resulting in $d = 3.16$ and $d = 3.22 \text{ \AA}$, respectively. Our calculated radial distribution functions (RDFs) of Cu–Cu and Co–Co distances, Figure S2, show prominent broad peaks with maxima at ~ 4.0 and $\sim 4.3 \text{ \AA}$ for Cu and Co, respectively.

As schematically depicted on the top row of Figure 2, we characterize three classes of movements outlined as follows: (i) movement of layers in the xy plane leading to slipped layers; (ii) a vertical movement of layers in the z direction; and (iii) deformation of organic linkers leading to rippled layers. Figure 2a,b illustrates the slipping motion of six adjacent layers of $\text{Co}_3(\text{HHTP})_2$, upper row, and $\text{Cu}_3(\text{HHTP})_2$, lower row, during the last 500 ps of an entire 3 ns NPT simulation using the positions of six representative metal nodes in those layers as geometrical indicators. Slipping of layers, mostly to form an AB slipped-parallel stacking pattern, has been confirmed in various 2D MOFs via a combination of experimental and theoretical PXRD analyses.^{12,13,20,27,29,69} Our MD simulations of $\text{Co}_3(\text{HHTP})$ confirm this stacking pattern where the layers alternatively slip in the opposite directions in the xy plane as seen in Figure 2a,b. However, we do not see the exact same stacking pattern for $\text{Cu}_3(\text{HHTP})_2$. Instead, the observed pattern for $\text{Cu}_3(\text{HHTP})_2$ in Figure 2a reminds us of recent experimental results which showed in the x direction, out of four layers, three are stacked with an offset along the same direction, while the forth layer is stacked with an offset in the opposite direction, overall representing a stacking fault.⁷⁰ Furthermore, Figure 2a,b shows that the movement of layers is a constant motion where, after forming the slipped-parallel stacking, the layers can still move up to $\sim 2 \text{ \AA}$ in x or y directions. Figure 2c illustrates the vertical motion of six adjacent layers of $\text{Co}_3(\text{HHTP})_2$ and $\text{Cu}_3(\text{HHTP})_2$ during the last 500 ps of the NPT simulation. As can be clearly seen, even after equilibration, the layers are still constantly moving along the z direction which in the case of $\text{Cu}_3(\text{HHTP})_2$ looks more pronounced and correlated than the $\text{Co}_3(\text{HHTP})_2$ MOF. The constant deformations of organic linkers are depicted in Figure 2d using positions of the three metal sites, connected to the

same organic linker, in the z direction as the geometrical indicator. We show the first 100 ps of the equilibration stage in order to emphasize that the organic linker is planar in the beginning of the simulation; hence, all three metal nodes share similar z coordinates. As the simulation starts, one metal node moves in the direction opposite to the other two thereby twisting the organic linker. As shown in the last 100 ps of the simulation, linker deformation never stops at the studied 293 K temperature and 1 atm pressure, as the metal nodes, despite being on the same layer, have different positions in the z direction.

Intrinsic Structural Deformations. A close examination of the MD equilibrated systems for the dry $\text{Co}_3(\text{HHTP})_2$ and $\text{Cu}_3(\text{HHTP})_2$ MOFs at 293 K and 1 atm reveals two different coordination environments. Beside nearly square planar metal (M) centers, one can also find a second form of coordination environment with (pseudo)tetrahedral configuration. The C–C–O–M dihedral angle is 180° in an ideal square planar complex, allowing full conjugation of the oxo groups of the organic linkers with benzene rings and their full electron donations to the M^{2+} centers. On the other hand, the approximate range of 80 – 170° C–C–O–M dihedral angles in the (pseudo)tetrahedral M sites weakens the coordinative M–O bonds. We elect to call these M sites, with (pseudo)-tetrahedral arrangements and deformed linkers, *intrinsic deformation sites*. To gain further insights, restrained electrostatic potential (RESP) charges⁷¹ were calculated at the PBE-D3/DZVP-MOLOPT level using the final snapshot of the 3 ns MD equilibrated $\text{Co}_3(\text{HHTP})_2$ MOF.

As can be seen from Figure 3, these *intrinsic deformation sites* in $\text{Co}_3(\text{HHTP})_2$ are in average $\sim 0.2 \text{ e}$ more positively charged than the square planar Co sites, which eludes to their possible higher susceptibility to nucleophilic attacks from confined water molecules. Here, we emphasize that characterization of these intrinsic deformation sites in $\text{Co}_3(\text{HHTP})_2$ and $\text{Cu}_3(\text{HHTP})_2$ is based on our MD simulations at 293 K temperature and 1 atm pressure. Keeping in mind the flexible nature of these layered materials where weak van der Waals interactions allow the rippling, slipping, and breathing motions of the layers, one may expect that the two coordination environments are metastable, with different relative stabilities depending on environmental conditions.

Water Adsorption: Thermodynamical View. While water molecules can form coordinative bonds with open-metal sites in 2D MOFs, they can also donate hydrogen bonds

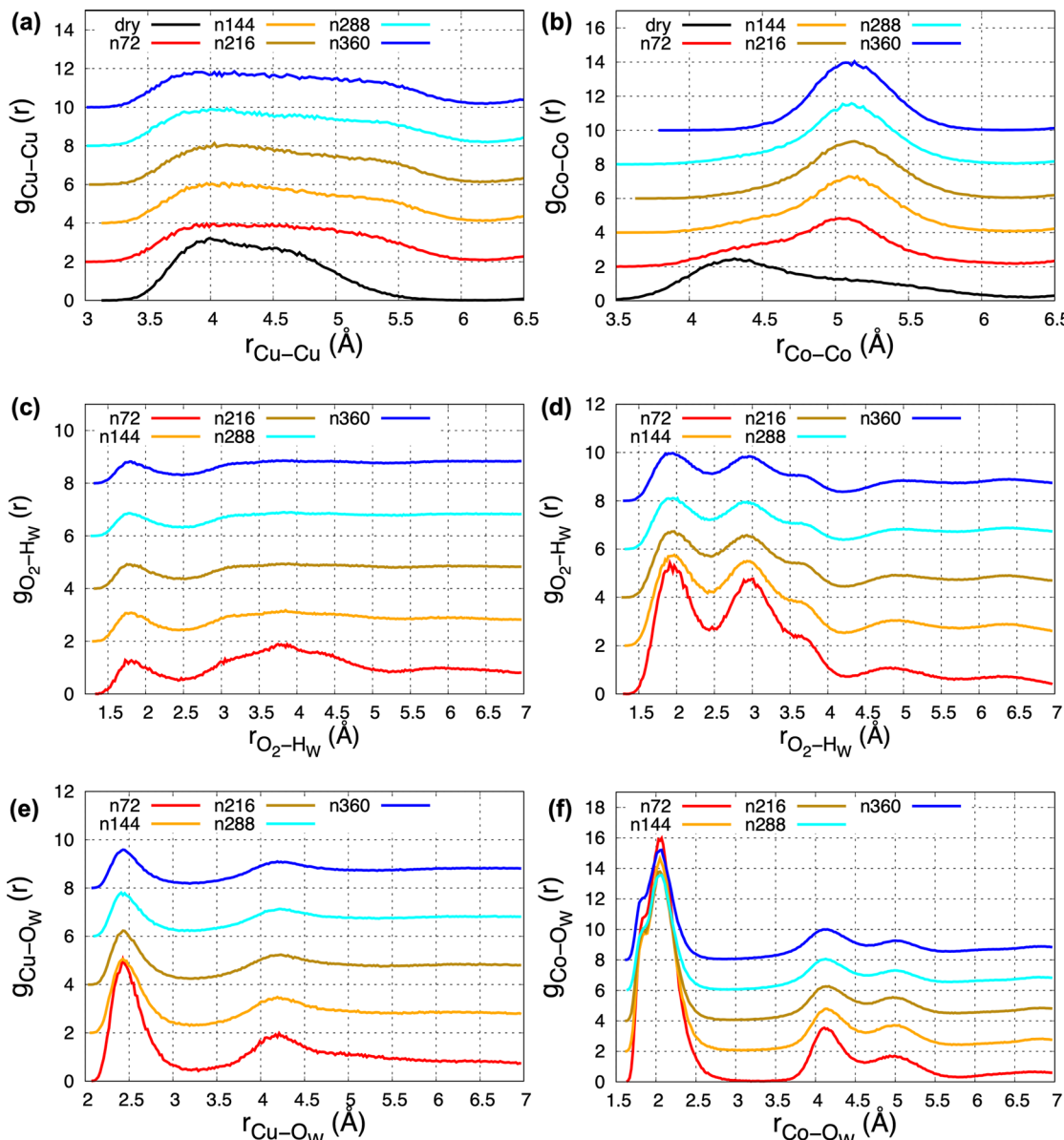


Figure 4. Calculated M–M, representative O_2-H_W (hydrogen of water) and M– O_w (oxygen of water) RDFs for M = Cu (a, c, e, left column) and M = Co (b, d, f, right column) systems. All calculated RDFs are shifted by two units for better clarity.

to the oxo groups of the HHTP linkers. To differentiate between different adsorption sites for water and to find the optimal concentration of water within the main 1D channels that would allow us to observe the existence of any differences between $Co_3(HHTP)_2$ and $Cu_3(HHTP)_2$, we ran a total of up to 2 ns NPT simulations on hydrated MOFs with different water loadings starting from their corresponding dry equilibrated systems. Each 1D channel in a $2 \times 2 \times 3$ super cell exposes $n = 36$ open-metal sites to the confined water. So, we elected to pack $2n = 72$, $4n = 144$, $6n = 216$, $8n = 288$, and $10n = 360$ water molecules. Extensive simulations were performed on different water packed configurations in both $Co_3(HHTP)_2$ and $Cu_3(HHTP)_2$ and the most stable configurations were selected for each water loaded framework.

Figure 4a,b illustrate the Cu–Cu and Co–Co RDFs in hydrated MOFs in comparison to dry MOFs shown in black. A very distinctive feature of the Co–Co RDFs is the shift of the maximum from ~ 4.3 Å in dry MOF to ~ 5.1 Å in hydrated

MOFs. This can be an indicative of water diffusion to the interlayer space and coordinating to the open-Co sites that forces an increase of the interlayer distance. Cu–Cu RDFs also show this phenomenon albeit to a lesser extent. While the maximum of the peak shifts from ~ 4 to ~ 4.25 Å, a shoulder also appears at ~ 5.25 Å. All studied water contents preserve the main peak and the shoulder which can be inferred as less affinity of water for inserting to the interlayer space and coordination to the open-Cu centers compared to the Co sites. Better insights into the mechanism of water adsorption by the two MOFs can be obtained through the analysis of the O_2-H_W , i.e., oxygen of the HHTP linker and hydrogen of water (Figure 4c,d), as well as M– O_w , i.e., metal center and oxygen of water (Figure 4e,f), RDFs. We suggest that adsorption through hydrogen bond formation with the oxo groups of the HHTP organic linkers can be considered as the primary mode of adsorption since there are twice as many oxo groups as metal centers in the 1D channel. They are also more exposed

and well-oriented toward the 1D channel and the confined water molecules than the open-metal sites. Perhaps even more importantly, their interactions with the water molecules do not require any significant structural changes as opposed to the coordination to the open-metal site which does require weakening of the vdW interactions in order to allow water molecules to diffuse into the interlayer space and form a coordination bond. The O₂–H_W peaks are relatively taller and sharper in the hydrated Co systems than Cu which signals that water is more structured in the former than the latter. Investigation of the M–O_W RDFs in Figure 4e,f clearly shows the first and second solvation shells in both MOFs. The stark difference between Cu₃(HHTP)₂ and Co₃(HHTP)₂ RDFs comes from the first peak which is shorter by ~0.4 Å in the latter than the former for all studied water contents showing the higher tendency of the Co system to adsorb water as compared to Cu. As can be seen from Figure 4f, a shoulder also appears in the calculated Co–O_W RDFs for all water contents. Analyses of our MD trajectories show that this shoulder with shorter bond distances corresponds to the water molecules that are coordinated to Co sites only bonded to one HHTP organic linker.

To shed more light on the affinity of each system toward adsorbing water, we calculated enthalpy of adsorption (ΔH_{ads}) per water molecule in both Cu₃(HHTP)₂ and Co₃(HHTP)₂ for different water contents using the following equation:

$$\Delta H_{\text{ads}} = \frac{1}{n} [E_{n@{\text{MOF}}} - E_{\text{MOF}} - (n \times E_{\text{wat}})] \quad (1)$$

where E_{MOF} and $E_{n@{\text{MOF}}}$ refer to the configurational energy of the dry and hydrated MOFs with n being the number of water molecules, and E_{wat} is the energy of a single q-TIP4P/F water molecule. The computed ΔH_{ads} values at all water contents show the higher tendency of Co₃(HHTP)₂ for adsorbing water molecules compared to Cu₃(HHTP)₂ (e.g., $\Delta H_{\text{ads}} = -20.8$ vs -10.2 kcal/mol in 72@MOFs, Figure 5).

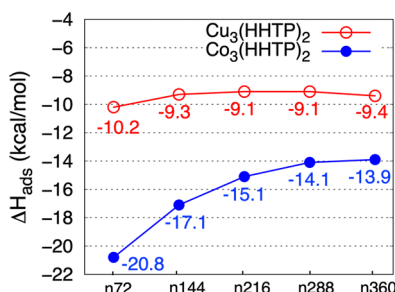


Figure 5. Computed enthalpy of adsorption of water in Cu₃(HHTP)₂, in red, and Co₃(HHTP)₂, in blue, at different water loadings.

As the water content increases, the computed ΔH_{ads} values of Cu₃(HHTP)₂ and Co₃(HHTP)₂ both reach an almost plateau value though Co₃(HHTP)₂ still shows higher enthalpy of adsorption per water molecule than its Cu counterpart. For comparison, recently the ΔH_{ads} per water molecules for the zeolitic imidazolate framework-90, which is generally classified as a hydrophilic material, is calculated to be ~−11 kcal/mol.⁷² Overall, adsorption of water leads to formation of water coordinated complexes and partial hydrolysis of the layers in the Co₃(HHTP)₂ 2D MOF with most Co centers accepting two or more water molecules. This also increases the interlayer

distances which weakens the interlayer van der Waals interactions in the framework. On the other hand, the metal centers of the Cu₃(HHTP)₂ 2D MOF show a lesser tendency for adsorbing water, accepting none or only one. This is consistent with the lower ΔH_{ads} of the Cu₃(HHTP)₂ 2D MOF as reported in Figure 5.

Binding Affinity of the Open-Metal Sites to Water vs the Organic Linkers. To gain more insights into water stability of the 2D Co₃(HHTP)₂ and Cu₃(HHTP)₂ MOFs, we performed highly accurate ωB97M-v/def2-TZVP quantum-mechanical calculations and obtained the change in Gibbs free energy and enthalpy for step by step addition of catocalate (CAT) ligands and water molecules to metal centers to form two different metal nodes we observed from our MD simulations. As shown in Figure 6, we call these nodes *bridging* SBU and *hydrolyzed* SBU. As can be seen from Figure 6, Cu²⁺ generally has a higher affinity for organic linkers than Co²⁺. On the other hand, Co²⁺ has a higher affinity for water molecules, let it be addition of two water molecules to form *bridging* SBU or addition of all four water molecules to form *hydrolyzed* SBU. Additions of the first and second CAT linkers to both Co²⁺ and Cu²⁺ are expectedly very exothermic; however, they are −29.2 and −14.9 kcal/mol more exothermic for the latter than the former. On the other hand, the first and second water additions to the M(CAT)₂ complexes are −8.4 and −10.8 kcal/mol more exothermic in the case of Co²⁺ compared to Cu²⁺ (left side of Figure 6). Interestingly, the addition of the second water to Cu(CAT)₂(H₂O) to form the bridging SBU is slightly endothermic by +0.8 kcal/mol (left side of Figure 6). This sheds light on the water chemisorption behavior of the Cu₃(HHTP)₂ MOF and agrees with our MD simulations where, except a few, all Cu²⁺ metal centers were found to prefer to adsorb no or only one water molecule.

Similarly, while the addition of the first water molecule to Cu(CAT)⁺ is more exothermic than Co(CAT)⁺ by −14.9 kcal/mol (right side of Figure 6) the addition of the second water is the bottleneck of the reaction with calculated $\Delta G = -0.3$ kcal/mol for Cu(CAT)(H₂O)⁺ compared to −26.8 kcal/mol for Co(CAT)(H₂O)⁺. A close inspection of the final Cu(CAT)(H₂O)⁺ complex, at the bottom of Figure 6, shows that this complex is formed by a network of hydrogen bonded water molecules rather than coordination of water molecules to the metal center. On the other hand, Co²⁺ centers are able to accept more than one water molecule exothermically all the way until a perfect octahedral complex is formed. Overall, our highly accurate quantum-mechanical calculations presented here confirm that formations of both *bridging* and *hydrolyzed* SBUs are thermodynamically favorable in the case of the Co₃(HHTP)₂ MOF. It is also worthwhile mentioning that the computed Cu–O_W and Co–O_W bond lengths from our quantum-mechanical calculations for the *bridging* SBU isomers are in relatively good agreement with their corresponding computed RDFs from the MD simulations (Figure 6 vs Figure 5e,f).

Water Adsorption: Dynamical View. To gain further insights into the dynamical properties of the confined water, we calculated water reorientation relaxation times as well as diffusion coefficients over an ensemble of 10 independent microcanonical NVE trajectories, each with a duration of 50 ps starting from randomly generated configurations using trajectories from our 10 ps canonical NVT ensemble simulations. We calculated the total diffusion coefficient

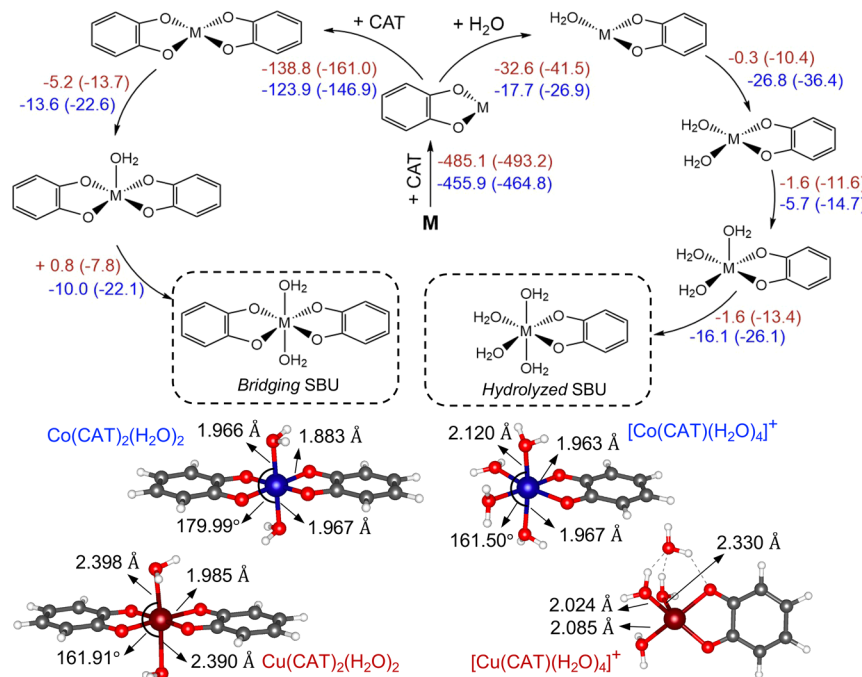


Figure 6. ω B97M-v/def2-TZVP computed changes in Gibbs free energy and enthalpy (in parentheses) for addition of the CAT linkers and water molecules to $M = \text{Cu}^{2+}$ (red) and $M = \text{Co}^{2+}$ (blue) metal centers. M06-L optimized structures of final products with their key bond lengths and angles are also given.

Table 1. Computed Water Reorientation Relaxation Time (τ_{reor} in ps), Total Diffusion Coefficients (D_{tot}), and Diffusion Coefficients along the xy Plane (D_{xy}) and z Direction (D_z) in $\text{\AA}^2 \text{ps}^{-1}$ for $\text{Cu}_3(\text{HHTP})_2$ and $\text{Co}_3(\text{HHTP})_2$ MOFs with Different Water Contents^a

n	$\text{Cu}_3(\text{HHTP})_2$			$\text{Co}_3(\text{HHTP})_2$				
	τ_{reor}	D_{tot}	D_{xy}	D_z	τ_{reor}	D_{tot}	D_{xy}	D_z
72	55.3	0.032	0.020	0.054	107.1	0.003	0.002	0.006
144	44.3	0.039	0.032	0.054	99.3	0.013	0.009	0.021
216	34.0	0.046	0.038	0.060	76.3	0.024	0.016	0.038
288	31.1	0.049	0.042	0.062	59.9	0.025	0.018	0.037
360	21.5	0.048	0.043	0.058	54.1	0.027	0.021	0.039
exp.	1.7–2.6 ^{36–38}	0.229 ⁷⁶						
simul.	2.83	0.192						

^aFor comparison, experimental (exp.) and our MD simulated (simul.) values for bulk water at 298 K are also given.

(D_{tot}) based on mean square displacement (MSD) of the particles⁷³ as follows:

$$D = \lim_{t \rightarrow \infty} \frac{1}{6t} \langle (\mathbf{r}(t) - \mathbf{r}(0))^2 \rangle \quad (2)$$

Diffusion coefficients in the xy plane, i.e., into the interlayer space, as well as along the z direction, i.e., alongside the main 1D channels, were also calculated for all different water loadings. After plotting log MSD vs log time for all different water contents (Figure S13), the linear segments of the MSD data were used in these calculations.⁷⁴

We quantified water reorientation relaxation in terms of the orientational time correlation functions (TCFs); see Figure S12 for TCFs of different water contents in 2D MOFs. We formulated TCFs in terms of the reorientation of the unit vector $\hat{\mathbf{u}}_{\text{OH}}$ that lies along one of the OH bonds of a water molecule:

$$C_{2,\text{OH}}(t) = \langle P_2[\hat{\mathbf{u}}_{\text{OH}}(0) \cdot \hat{\mathbf{u}}_{\text{OH}}(t)] \rangle \quad (3)$$

where P_2 is the Legendre polynomial of order 2. To determine water reorientation relaxation times (τ_{reor}), we fitted the correlation function ensemble averaged over all water molecules over time to a biexponential function⁷⁵ of the form

$$C_{2,\text{OH}}(t) = \left[a \times \exp\left(-\frac{t}{\tau_1}\right) \right] + \left[b \times \exp\left(-\frac{t}{\tau_2}\right) \right] \quad (4)$$

The final reorientation relaxation times were then calculated from the weighted average of the fitting parameters:

$$\tau_{\text{reor}} = \frac{(a \times \tau_1) + (b \times \tau_2)}{(a + b)} \quad (5)$$

The correlation functions were also fitted to a triexponential function of a similar form which yielded similar trends. For example in the case of the Cu MOF with $n = 216$ water molecules, a biexponential fit yielded a τ_{reor} value of 34.0 ps, and a triexponential fit resulted in a similar value of 36.2 ps. The first 100 fs which corresponds to the fast librational

motion of the water molecules⁷⁵ was excluded from these fits (see Figure S12).

Table 1 summarizes the calculated relaxation times and diffusion coefficients for five different water contents in both Cu₃(HHTP)₂ and Co₃(HHTP)₂ 2D MOFs; the corresponding experimental and simulated data for bulk water are also given for comparison.

The very high value of τ_{reor} for 72@Co₃(HHTP)₂, 107.1 ps, compared to 55.3 ps for 72@Cu₃(HHTP)₂ is in line with our computed ΔH_{ads} values, pointing to the higher interaction of water with the surface of the former system than the latter. As expected, increasing water content adds more bulk-like behavior to confined water in both MOFs resulting in a decrease in the computed reorientation relaxation times and an increase in the computed diffusion coefficients. Water is found to have a lower mobility alongside the interlayer spaces than along the main 1D channels in both studied Cu and Co MOFs, i.e., lower D_{xy} values than D_z (Table 1). Our calculated diffusion coefficients and reorientation relaxation times agree with our established higher tendency for the Co₃(HHTP)₂ 2D MOF compared to the Cu₃(HHTP)₂ framework to adsorb and *keep* water molecules. Overall, based on all of our simulations, we propose a four stage scenario for the behavior of confined water in 2D MOFs: (i) diffusion without a major hindrance along the main 1D channel; (ii) being drifted aside by first oxo groups of the HHTP linkers and then the open-metal sites; (iii) forming coordination bonds with the metal nodes and acting as nucleation sites to draw more water molecules to the interlayer space; (iv) and finally being pushed out to the nearby channels.

The overall structural integrity of Co₃(HHTP)₂ is preserved in aqueous solutions, but one may expect that hydrolysis will destroy the extended π - π conjugation and lower electrical conductivity, the highest merit of 2D MOFs in comparison with their conventional ancestors. Thus, we hope that this work inspires devising new strategies for increasing the water stability of 2D MOFs for preserving/increasing their conductivity. Overall, we envisage that one can modify the framework, the aqueous solution, or both to reduce the extent of interaction of metal nodes with incoming water molecules. Examples can be introducing hydrophobic alkyl, phenyl, or halogen substituents on organic linkers^{77–79} that keep water inside the channel, or replacing the oxo groups with amino and aminoalkyl groups to prevent formation of water clusters around metal nodes. Adding concentrated ionic solutions to water might also make it less invasive toward metal nodes of these frameworks as anomalous water diffusion in salt solutions is a known phenomenon.^{80,81}

CONCLUSIONS

2D layered MOFs are a new class of materials that offer electrical conductivity in addition to exceptional high surface area and permanent porosity of conventional MOFs with potential breakthrough applications. Engineering any structure-application relationships is a formidable challenge due to the lack of understanding of the intrinsic structure and dynamics of these intriguing systems. *Static* electronic structure calculations result in a too-perfect crystal structure which makes them inapplicable for studying the highly flexible π -stacked layered 2D MOFs. On the other hand, *ab initio* molecular dynamics simulations are prohibitively expensive to be performed long enough to reproduce their flexibility and structural dynamics especially when an interface with water as

solvent is to be considered and investigated. Here, we developed *ab initio* force fields (AIFFs) that allow simulation of a supercell comprised of 1512 atoms for rather long simulation times with reasonable accuracy. Our developed AIFFs reproduce the AB slipped-parallel stacking pattern of 2D MOFs as has been reported by recent experimental data. Molecular dynamics simulations at 293 K temperature and 1 atm pressure reveal the presence of two different coordination environments around metal (M) sites, one with M sites bridging two HHTP linkers and another with M sites connecting three organic linkers instead. Subsequent MD simulations in the presence of explicit water molecules along with accurate quantum-mechanical calculations for forming both the *bridging* and *hydrolyzed* SBUs show that the existence of *intrinsic deformation sites* together with the higher tendency of Co compared to Cu to adsorb water leads to partial hydrolysis of the Co₃(HHTP)₂ layers which agrees well with available experimental data. Our ω B97M-v calculated changes in Gibbs free energy show that Cu²⁺ has a low tendency toward coordination to water where addition of more than one water molecule was found to be endothermic. Co²⁺ on the other hand, was shown to readily accept water molecules for forming either *bridging* and/or *hydrolyzed* SBUs. The multifaceted approach introduced in this work constitutes a preliminary step on studying the intrinsic structure and dynamical nature of flexible layered 2D MOFs and its effect on stability and chemical reactivity of the metal nodes in aqueous solutions. Based on the current framework of MD simulations of confined water in flexible 2D MOFs, future directions should focus on (1) exploring the effects of nuclear quantum effects on the dynamical properties of the confined water in flexible layered MOFs, which is possible, for instance, through ring polymer molecular dynamics (RPMD) simulations, and (2) refining the developed AIFFs by adding new parameters to incorporate interlayer van der Waals interactions.

ASSOCIATED CONTENT

Supporting Information

The Supporting Information is available free of charge at <https://pubs.acs.org/doi/10.1021/acs.chemmater.2c00989>.

Details of our flexible *ab initio* force fields, periodic and cluster electronic structure calculations, classical MD simulations, calculated mean square displacements, and orientational relaxation time correlation functions (PDF)

Input (CONFIG, CONTROL, and FIELD) and output (REVCON, STATIS, and OUTPUT) files of the MD simulations (ZIP)

XYZ coordinates (ZIP)

AUTHOR INFORMATION

Corresponding Authors

Mohammad R. Momeni – Department of Chemistry and Environmental Science, New Jersey Institute of Technology, Newark 07102 New Jersey, United States;  orcid.org/0000-0002-7731-5823; Email: momeni@njit.edu

Farnaz A. Shakib – Department of Chemistry and Environmental Science, New Jersey Institute of Technology, Newark 07102 New Jersey, United States;  orcid.org/0000-0003-1432-2812; Email: shakib@njit.edu

Authors

Yuliang Shi — Department of Chemistry and Environmental Science, New Jersey Institute of Technology, Newark 07102 New Jersey, United States

Yen-Jui Chen — Department of Chemistry and Environmental Science, New Jersey Institute of Technology, Newark 07102 New Jersey, United States

Dil K. Limbu — Department of Chemistry and Environmental Science, New Jersey Institute of Technology, Newark 07102 New Jersey, United States; orcid.org/0000-0001-9196-9498

Zeyu Zhang — Department of Chemistry and Environmental Science, New Jersey Institute of Technology, Newark 07102 New Jersey, United States

Complete contact information is available at:

<https://pubs.acs.org/10.1021/acs.chemmater.2c00989>

Author Contributions

The authors have no conflicts of interest to declare.

Notes

The authors declare no competing financial interest.

Data Availability. The data that support the findings of this study are available in the paper and the [Supporting Information](#). Additional data are available from the corresponding authors upon reasonable request.

ACKNOWLEDGMENTS

This work is supported by start-up fund from New Jersey Institute of Technology (NJIT) and used the Extreme Science and Engineering Discovery Environment (XSEDE), which is supported by National Science Foundation grant number CHE200007. This research has been partially enabled by the use of computing resources and support provided by the HPC center at NJIT.

REFERENCES

- (1) Geim, A.; Novoselov, K. The rise of graphene. *Nat. Mater.* **2007**, *6*, 183–191.
- (2) Geim, A. Graphene: status and prospects. *Science* **2009**, *324*, 1530–1534.
- (3) Huang, X.; Yin, Z.; Wu, S.; Qi, X.; He, Q.; Zhang, Q.; Yan, Q.; Boey, F.; Zhang, H. Graphene-based materials: synthesis, characterization, properties, and applications. *Small* **2011**, *7*, 1876.
- (4) Novoselov, K.; Fal'ko, V.; Colombo, L.; Gellert, P.; Schwab, M. G.; Kim, K. A roadmap for graphene. *Nature* **2012**, *490*, 192–200.
- (5) Gunjakar, J.; Kim, I.; Lee, J.; Jo, Y.; Hwang, S.-J. Exploration of nanostructured functional materials based on hybridization of inorganic 2D nanosheets. *J. Phys. Chem. C* **2014**, *118*, 3847–3863.
- (6) Ko, M.; Mendecki, L.; Mirica, K. Conductive two-dimensional metal–organic frameworks as multifunctional materials. *Chem. Commun.* **2018**, *54*, 7873–7891.
- (7) Huang, C.; Li, Y.; Wang, N.; Xue, Y.; Zuo, Z.; Liu, H.; Li, Y. Progress in research into 2D graphdiyne-based materials. *Chem. Rev.* **2018**, *118*, 7744–7803.
- (8) Choudhuri, I.; Bhauriyal, P.; Pathak, B. Recent advances in graphene-like 2D materials for spintronics applications. *Chem. Mater.* **2019**, *31*, 8260–8285.
- (9) Hmadeh, M.; et al. New porous crystals of extended metalcatecholates. *Chem. Mater.* **2012**, *24*, 3511–3513.
- (10) Huang, X.; Sheng, P.; Tu, Z.; Zhang, F.; Wang, J.; Geng, H.; Zou, Y.; Di, C.-A.; Yi, Y.; Sun, Y.; Zhu, D. Two-dimensional π -d conjugated coordination polymer with extremely high electrical conductivity and ambipolar transport behavior. *Nat. Commun.* **2015**, *6*, 7408.
- (11) Sun, L.; Campbell, M.; Dincă, M. Electrically conductive porous metal-organic frameworks. *Angew. Chem., Int. Ed.* **2016**, *55*, 3566–3579.
- (12) Clough, A.; Skelton, J.; Downes, C.; de la Rosa, A.; Yoo, J.; Walsh, A.; Melot, B.; Marinescu, S. Metallic conductivity in a two-dimensional cobalt dithiolene metal-organic framework. *J. Am. Chem. Soc.* **2017**, *139*, 10863–10867.
- (13) Dou, J.-H.; Sun, L.; Ge, Y.; Li, W.; Hendon, C.; Li, J.; Gul, S.; Yano, J.; Stach, E.; Dincă, M. Signature of Metallic Behavior in the Metal-Organic Frameworks $M_3(\text{Hexaiminobenzene})_2$ ($M = \text{Ni}, \text{Cu}$). *J. Am. Chem. Soc.* **2017**, *139*, 13608–13611.
- (14) Corma, A.; García, H.; Llabrés i Xamena, F. X. Engineering Metal Organic Frameworks for Heterogeneous Catalysis. *Chem. Rev.* **2010**, *110*, 4606–4655.
- (15) Farha, O. K.; Hupp, J. T. Rational Design, Synthesis, Purification, and Activation of Metal-Organic Framework Materials. *Acc. Chem. Res.* **2010**, *43*, 1166–1175.
- (16) Furukawa, H.; Cordova, K. E.; O'Keeffe, M.; Yaghi, O. M. The Chemistry and Applications of Metal-Organic Frameworks. *Science* **2013**, *341*, 1230444.
- (17) Sheberla, D.; Sun, L.; Blood-Forsythe, M.; Er, S.; Wade, C.; Brozek, C.; Aspuru-Guzik, A.; Dincă, M. High electrical conductivity in $\text{Ni}_3(2,3,6,7,10,11\text{-hexaiminotriphenylene})_2$, a semiconducting metal-organic graphene analogue. *J. Am. Chem. Soc.* **2014**, *136*, 8859–8862.
- (18) Wu, G.; Huang, J.; Zang, Y.; He, J.; Xu, G. Porous field-effect transistors based on a semiconductive metal-organic framework. *J. Am. Chem. Soc.* **2017**, *139*, 1360–1363.
- (19) Sheberla, D.; Bachman, J.; Elias, J.; Sun, C.-J.; Shao-Horn, Y.; Dincă, M. Conductive MOF electrodes for stable supercapacitors with high areal capacitance. *Nat. Mater.* **2017**, *16*, 220–224.
- (20) Li, W.-H.; Ding, K.; Tian, H.-R.; Yao, M.-S.; Nath, B.; Deng, W.-H.; Wang, Y.; Xu, G. Conductive metal-organic framework nanowire array electrodes for high-performance solid-state supercapacitors. *Adv. Funct. Mater.* **2017**, *27*, 1702067.
- (21) Sheberla, D.; Bachman, J.; Elias, J.; Sun, C.; Shao-Horn, Y.; Dincă, M. Conductive MOF electrodes for stable supercapacitors with high areal capacitance. *Nat. Mater.* **2017**, *16*, 220–224.
- (22) Feng, D.; et al. Robust and conductive two-dimensional metal-organic frameworks with exceptionally high volumetric and areal capacitance. *Nat. Energy* **2018**, *3*, 30–36.
- (23) Clough, A.; Yoo, J.; Mecklenburg, M.; Marinescu, S. Two-dimensional metal-organic surfaces for efficient hydrogen evolution from water. *J. Am. Chem. Soc.* **2015**, *137*, 118–121.
- (24) Dong, R.; Pfeffermann, M.; Liang, H.; Zheng, Z.; Zhu, X.; Zhang, J.; Feng, X. Large-area, free-standing, two-dimensional supramolecular polymer single-layer sheets for highly efficient electrocatalytic hydrogen evolution. *Angew. Chem., Int. Ed.* **2015**, *54*, 12058–12063.
- (25) Miner, E.; Fukushima, T.; Sheberla, D.; Sun, L.; Surendranath, Y.; Dincă, M. Electrochemical oxygen reduction catalysed by $\text{Ni}_3(\text{hexaiminotriphenylene})_2$. *Nat. Commun.* **2016**, *7*, 10942.
- (26) Huang, X.; Yao, H.; Cui, Y.; Hao, W.; Zhu, J.; Xu, W.; Zhu, D. Conductive copper benzenehexathiol coordination polymer as a hydrogen evolution catalyst. *ACS Appl. Mater. Interfaces* **2017**, *9*, 40752–40759.
- (27) Sun, X.; Wu, K.-H.; Sakamoto, R.; Kusamoto, T.; Maeda, H.; Ni, X.; Jiang, W.; Liu, F.; Sasaki, S.; Masunaga, H.; Nishihara, H. Bis(aminothiolato)nickel nanosheet as a redox switch for conductivity and an electrocatalyst for the hydrogen evolution reaction. *Chem. Sci.* **2017**, *8*, 8078–8085.
- (28) Mendecki, L.; Ko, M.; Zhang, X.; Meng, Z.; Mirica, K. Porous scaffolds for electrochemically controlled reversible capture and release of ethylene. *J. Am. Chem. Soc.* **2017**, *139*, 17229–17232.
- (29) Yao, M.; Lv, X.; Fu, Z.; Li, W.; Deng, W.; Wu, G.; Xu, G. Layer-by-layer assembled conductive metal-organic framework nanofilms for room-temperature chemiresistive sensing. *Angew. Chem., Int. Ed.* **2017**, *56*, 16510–16514.

- (30) Mendecki, L.; Mirica, K. Conductive metal–organic frameworks as ion-to-electron transducers in potentiometric sensors. *ACS Appl. Mater. Interfaces* **2018**, *10*, 19248–19257.
- (31) Jia, H.; Yao, Y.; Zhao, J.; Gao, Y.; Luo, Z.; Du, P. Novel two-dimensional nickel phthalocyanine-based metal–organic framework for highly efficient water oxidation catalysis. *J. Mater. Chem. A* **2018**, *6*, 1188–1195.
- (32) Downes, C.; Clough, A.; Chen, K.; Yoo, J.; Marinescu, S. Evaluation of the H_2 evolving activity of benzenehexathiolate coordination frameworks and the effect of film thickness on H_2 production. *ACS Appl. Mater. Interfaces* **2018**, *10*, 1719–1727.
- (33) Meng, Z.; Aykanat, A.; Mirica, K. Welding metallocphthalocyanines into bimetallic molecular meshes for ultra-sensitive, low-power chemiresistive detection of gases. *J. Am. Chem. Soc.* **2019**, *141*, 2046–2053.
- (34) Foster, M.; Sohlberg, K.; Spataru, C.; Allendorf, M. Proposed modification of the graphene analogue $Ni_3(HITP)_2$ to yield a semiconducting material. *J. Phys. Chem. C* **2016**, *120*, 15001–15008.
- (35) Foster, M.; Sohlberg, K.; Allendorf, M.; Talin, A. Unraveling the semiconducting/metallic discrepancy in $Ni_3(HITP)_2$. *J. Phys. Chem. Lett.* **2018**, *9*, 481–486.
- (36) Winkler, K.; Lindner, J.; Büsing, H.; Vöhringer, P. Ultrafast Raman-induced Kerr-effect of water: Single molecule versus collective motions. *J. Chem. Phys.* **2000**, *113*, 4674.
- (37) Lawrence, C. P.; Skinner, J. L. Vibrational spectroscopy of HOD in liquid D₂O. D 2 O. III. Spectral diffusion, and hydrogen-bonding and rotational dynamics. *J. Chem. Phys.* **2003**, *118*, 264.
- (38) Rezus, Y. L. A.; Bakker, H. J. On the orientational relaxation of HDO in liquid water. *J. Chem. Phys.* **2005**, *123*, 114502.
- (39) Hummer, G.; Rasaiah, J. C.; Noworyta, J. P. Water conduction through the hydrophobic channel of a carbon nanotube. *Nature* **2001**, *414*, 188–190.
- (40) Vaiteeswaran, S.; Rasaiah, J. C.; Hummer, G. Electric field and temperature effects on water in the narrow nonpolar pores of carbon nanotubes. *J. Chem. Phys.* **2004**, *121*, 7955–7965.
- (41) Ortiz, A. U.; Freitas, A. P.; Boutin, A.; Fuchs, A. H.; Coudert, F.-X. What makes zeolitic imidazolate frameworks hydrophobic or hydrophilic? The impact of geometry and functionalization on water adsorption. *Phys. Chem. Chem. Phys.* **2014**, *16*, 9940–9949.
- (42) Calero, S.; Gómez-Álvarez, P. Underlying Adsorption Mechanisms of Water in Hydrophobic and Hydrophilic Zeolite Imidazolate Frameworks: ZIF-71 and ZIF-90. *J. Phys. Chem. C* **2015**, *119*, 23774–23780.
- (43) Haigis, V.; Coudert, F.-X.; Vuilleumier, R.; Boutin, A. Investigation of structure and dynamics of the hydrated metal–organic framework MIL-53(Cr) using first-principles molecular dynamics. *Phys. Chem. Chem. Phys.* **2013**, *15*, 19049.
- (44) Boutin, A.; Bousquet, D.; Ortiz, A. U.; Coudert, F.-X.; Fuchs, A. H.; Ballandras, A.; Weber, G.; Bezverkhyy, I.; Bellat, J.-P.; Ortiz, G.; Chaplais, G.; Paillaud, J.-L.; Marichal, C.; Nouali, H.; Patarin, J. Temperature-Induced Structural Transitions in the Gallium-Based MIL-53 Metal–Organic Framework. *J. Phys. Chem. C* **2013**, *117*, 8180–8188.
- (45) Coudert, F.-X.; Ortiz, A. U.; Haigis, V.; Bousquet, D.; Fuchs, A. H.; Ballandras, A.; Weber, G.; Bezverkhyy, I.; Geoffroy, N.; Bellat, J.-P.; Ortiz, G.; Chaplais, G.; Patarin, J.; Boutin, A. Water Adsorption in Flexible Gallium-Based MIL-53 Metal–Organic Framework. *J. Phys. Chem. C* **2014**, *118*, 5397–5405.
- (46) Haigis, V.; Coudert, F.-X.; Vuilleumier, R.; Boutin, A.; Fuchs, A. H. Hydrothermal Breakdown of Flexible Metal–Organic Frameworks: A Study by First-Principles Molecular Dynamics. *J. Phys. Chem. Lett.* **2015**, *6*, 4365–4370.
- (47) Vandichel, M.; Hajek, J.; Ghysels, A.; Vos, A. D.; Waroquier, M.; Speybroeck, V. V. Water coordination and dehydration processes in defective UiO-66 type metal organic frameworks. *CrystEngComm* **2016**, *18*, 7056–7069.
- (48) Lamaire, A.; Wieme, J.; Hoffman, A.; Speybroeck, V. V. Atomistic insight in the flexibility and heat transport properties of the stimuli-responsive metal–organic framework MIL-53(Al) for water-adsorption applications using molecular simulations. *Faraday Discuss.* **2020**, *225*, 301–323.
- (49) Burch, N. C.; Walton, I. M.; Hungerford, J. T.; Morelock, C. R.; Jiao, Y.; Heinen, J.; Chen, Y.-S.; Yakovenko, A. A.; Xu, W.; Dubbeldam, D.; Walton, K. S. I. *n* situ visualization of loading-dependent water effects in a stable metal–organic framework. *Nature Chem.* **2020**, *12*, 186–192.
- (50) Scalfi, L.; Fraux, G.; Boutin, A.; Coudert, F.-X. Structure and Dynamics of Water Confined in Imogolite Nanotubes. *Langmuir* **2018**, *34*, 6748–6756.
- (51) Perdew, J. P.; Burke, K.; Ernzerhoff, M. Erratum: Generalized gradient approximation made simple. *Phys. Rev. Lett.* **1997**, *78*, 1396–1396.
- (52) Grimme, S.; Antony, J.; Ehrlich, S.; Krieg, H. A consistent and accurate ab initio parametrization of density functional dispersion correction (DFT-D) for the 94 elements H–Pu. *J. Chem. Phys.* **2010**, *132*, 154104.
- (53) Hutter, J.; Iannuzzi, M.; Schiffmann, F.; VandeVondele, J. cp2k: atomistic simulations of condensed matter systems. *WIREs Computational Molecular Science* **2014**, *4*, 15–25.
- (54) Mardirossian, N.; Head-Gordon, M. ω B97M-V: A combinatorially optimized, range-separated hybrid, meta-GGA density functional with VV10 nonlocal correlation. *J. Chem. Phys.* **2016**, *144*, 214110.
- (55) Shao, Y.; Gan, Z.; Epifanovsky, E.; Gilbert, A. T.; Wormit, M.; Kussmann, J.; Lange, A. W.; Behn, A.; Deng, J.; Feng, X.; et al. Advances in molecular quantum chemistry contained in the Q-Chem 4 program package. *Mol. Phys.* **2015**, *113*, 184–215.
- (56) Goldberg, D. *Genetic Algorithms in Search, Optimization and Machine Learning*; Addison-Wesley: Boston, 1989.
- (57) Yang, G.; Reinstein, L. E.; Pai, S.; Xu, Z.; Carroll, D. L. A new genetic algorithm technique in optimization of permanent 125-I prostate implants. *Med Phys.* **1998**, *25*, 2308–2315.
- (58) Wang, J.; Wolf, R. M.; Caldwell, J. W.; Kollman, P. A.; Case, D. A. Development and testing of a general amber force field. *J. Computat. Chem.* **2004**, *25*, 1157–1174.
- (59) Momeni, M. R.; Shakib, F. A. *The DL_Poly Quantum molecular simulation package*. https://github.com/fashakib/DL_Poly-Quantum-v1.0.
- (60) Smith, W.; Forester, T. R.; Todorov, I. T. *The DL_Poly Classic molecular simulation package*; STFC Daresbury Laboratory. https://gitlab.com/DL_Poly_Classic.
- (61) Smith, W.; Forester, T. R. *DL_Poly_2.0*: A general-purpose parallel molecular dynamics simulation package. *J. Mol. Graph.* **1996**, *14*, 136–141.
- (62) Yoshida, H. Construction of higher order symplectic integrators. *Phys. Lett. A* **1990**, *150*, 262–268.
- (63) Suzuki, M. General theory of fractal path integrals with applications to many-body theories and statistical physics. *J. Math. Phys.* **1991**, *32*, 400–407.
- (64) Martyna, G. J.; Tuckerman, M. E.; Tobias, D. J.; Klein, M. L. Explicit reversible integrators for extended systems dynamics. *Mol. Phys.* **1996**, *87*, 1117–1157.
- (65) Martyna, G. J.; Tobias, D. J.; Klein, M. L. Constant pressure molecular dynamics algorithms. *J. Chem. Phys.* **1994**, *101*, 4177–4189.
- (66) Tuckerman, M. E.; Alejandre, J.; López-Rendón, R.; Jochim, A. L.; Martyna, G. J. A Liouville-operator derived measure-preserving integrator for molecular dynamics simulations in the isothermal–isobaric ensemble. *J. Phys. A: Math. Gen.* **2006**, *39*, 5629–5651.
- (67) Habershon, S.; Markland, T. E.; Manolopoulos, D. E. Competing quantum effects in the dynamics of a flexible water model. *J. Chem. Phys.* **2009**, *131*, 024501.
- (68) Martínez, L.; Andrade, R.; Birgin, E. G.; Martínez, J. M. PACKMOL: A package for building initial configurations for molecular dynamics simulations. *J. Comput. Chem.* **2009**, *30*, 2157–2164.
- (69) Li, W.; Sun, L.; Qi, J.; Jarillo-Herrero, P.; Dincă, M.; Li, J. High temperature ferromagnetism in π -conjugated two-dimensional metal–organic frameworks. *Chem. Sci.* **2017**, *8*, 2859–2867.

- (70) Day, R. W.; Bediako, D. K.; Rezaee, M.; Parent, L. R.; Skorupakii, G.; Arguilla, M. Q.; Hendon, C. H.; Stassen, I.; Gianneschi, N. C.; Kim, P.; Dincă, M. Single Crystals of Electrically Conductive Two-Dimensional Metal-Organic Frameworks: Structural and Electrical Transport Properties. *ACS Cent. Sci.* **2019**, *5*, 1959–1964.
- (71) Golze, D.; Hutter, J.; Iannuzzi, M. Wetting of water on hexagonal boron nitride@Rh(111): a QM/MM model based on atomic charges derived for nano-structured substrates. *Phys. Chem. Chem. Phys.* **2015**, *17*, 14307–14316.
- (72) Wagner, J. C.; Hunter, K. M.; Paesani, F.; Xiong, W. Water Capture Mechanisms at Zeolitic Imidazolate Framework Interfaces. *J. Am. Chem. Soc.* **2021**, *143*, 21189–21194.
- (73) Nitzan, A. *Chemical Dynamics in Condensed Phases: Relaxation, Transfer, and Reactions in Condensed Molecular Systems*; Oxford University Press: Oxford, 2006.
- (74) Maginn, E. J.; Messerly, R. A.; Carlson, D. J.; Roe, D. R.; Elliot, J. R. Best Practices for Computing Transport Properties 1. Self-Diffusivity and Viscosity from Equilibrium Molecular Dynamics. *Living J. Comp. Mol. Sci.* **2018**, *1*, 6324.
- (75) Kim, S.; Wang, X.; Jang, J.; Eom, K.; Clegg, S. L.; Park, G.-S.; Di Tommaso, D. Hydrogen-Bond Structure and Low-Frequency Dynamics of Electrolyte Solutions: Hydration Numbers from ab Initio Water Reorientation Dynamics and Dielectric Relaxation Spectroscopy. *ChemPhysChem* **2020**, *21*, 2334–2346.
- (76) Krynicki, K.; Green, C. D.; Sawyer, D. W. Pressure and temperature dependence of self-diffusion in water. *Faraday Discuss.* **1978**, *66*, 199.
- (77) Nguyen, J. G.; Cohen, S. M. Moisture-Resistant and Superhydrophobic Metal-Organic Frameworks Obtained via Post-synthetic Modification. *J. Am. Chem. Soc.* **2010**, *132*, 4560–4561.
- (78) Taylor, J. M.; Vaidhyanathan, R.; Iremonger, S. S.; Shimizu, G. K. H. Enhancing water stability of metal-organic frameworks via phosphonate monoester linkers. *J. Am. Chem. Soc.* **2012**, *134*, 14338–14340.
- (79) Serre, C. Superhydrophobicity in highly fluorinated porous metal-organic frameworks. *Angew. Chem., Int. Ed.* **2012**, *51*, 6048–6050.
- (80) Kim, J.; Wu, Z.; Morrow, A.; Yethiraj, A.; Yethiraj, A. Self-Diffusion and Viscosity in Electrolyte Solutions. *J. Phys. Chem. B* **2012**, *116*, 12007–12013.
- (81) Ding, Y.; Hassanali, A.; Parrinello, M. Anomalous water diffusion in salt solutions. *Proc. Natl. Acad. Sci. U.S.A.* **2014**, *111*, 3310–3315.